doi:10.1093/brain/awy143 BRAIN 2018: 141; 2032–2046 | 2032

BRAIN
A JOURNAL OF NEUROLOGY

Active role of capillary pericytes during stimulation-induced activity and spreading depolarization

Lila Khennouf,[1] Bodil Gesslein,[1] Alexey Brazhe,[1,2] J. Christopher Octeau,[3] Nikolay Kutuzov,[1] Baljit S. Khakh[3] and Martin Lauritzen[1,4]

Spreading depolarization is assumed to be the mechanism of migraine with aura, which is accompanied by an initial predominant hyperaemic response followed by persistent vasoconstriction. Cerebral blood flow responses are impaired in patients and in experimental animals after spreading depolarization. Understanding the regulation of cortical blood vessels during and after spreading depolarization could help patients with migraine attacks, but our knowledge of these vascular mechanisms is still incomplete. Recent findings show that control of cerebral blood flow does not only occur at the arteriole level but also at capillaries. Pericytes are vascular mural cells that can constrict or relax around capillaries, mediating local cerebral blood flow control. They participate in the constriction observed during brain ischaemia and might be involved the disruption of the microcirculation during spreading depolarization. To further understand the regulation of cerebral blood flow in spreading depolarization, we examined penetrating arterioles and capillaries with respect to vascular branching order, pericyte location and pericyte calcium responses during somatosensory stimulation and spreading depolarization. Mice expressing a red fluorescent indicator and intravenous injections of FITC-dextran were used to visualize pericytes and vessels, respectively, under two-photon microscopy. By engineering a genetically encoded calcium indicator we could record calcium changes in both pericytes around capillaries and vascular smooth muscle cells around arterioles. We show that somatosensory stimulation evoked a decrease in cytosolic calcium in pericytes located on dilating capillaries, up to the second order capillaries. Furthermore, we show that prolonged vasoconstriction following spreading depolarization is strongest in first order capillaries, with a persistent increase in pericyte calcium. We suggest that the persistence of the 'spreading cortical oligaemia' in migraine could be caused by this constriction of cortical capillaries. After spreading depolarization, somatosensory stimulation no longer evoked changes in capillary diameter and pericyte calcium. Thus, calcium changes in pericytes located on first order capillaries may be a key determinant in local blood flow control and a novel vascular mechanism in migraine. We suggest that prevention or treatment of capillary constriction in migraine with aura, which is an independent risk factor for stroke, may be clinically useful.

1 Department of Neuroscience and Center for Healthy Aging, University of Copenhagen, 2200 Copenhagen N, Denmark
2 Department of Biophysics, Faculty of Biology, Moscow State University, 119234 Moscow, Russia
3 Department of Physiology, David Geffen School of Medicine, University of California Los Angeles, Los Angeles, CA 90095-1751, USA
4 Department of Clinical Neurophysiology, Rigshospitalet, 2600 Glostrup, Denmark

Correspondence to: Martin Lauritzen
Nørre Allé 14
Mærsk Tower 07.04
2200 Copenhagen N, Denmark
E-mail: mlauritz@sund.dk

Keywords: cortical spreading depression; cerebral blood flow; migraine; aura

Received November 17, 2017. Revised April 5, 2018. Accepted April 7, 2018

Introduction

Spreading depolarization represents a massive failure of brain ion homeostasis, which propagates in the cerebral cortex with depolarization of neurons and astroglial cells (Leao, 1944; Sugaya *et al.*, 1975). In its mild form, spreading depolarization causes the aura in migraine patients, whereas in its severe form spreading depolarization may induce permanent damage of brain tissue (Dreier, 2016; Hartings *et al.*, 2017). Cerebral blood flow is reduced after spreading depolarization, with impaired functional hyperaemia and reduced stimulation-induced neuronal and glial calcium responses (Piilgaard and Lauritzen, 2009; Khennouf *et al.*, 2016), and these disturbances have also been observed in patients with migraine (Lauritzen, 1994). At the very start of migraine attacks, cerebral blood flow seems to first increase and then to decrease in the posterior part of the brain (Olesen *et al.*, 1981; Lauritzen *et al.*, 1983; Hadjikhani *et al.*, 2001). Subsequently, the low flow region, called spreading oligaemia, propagates into the parietal and temporal lobes at a rate of 2 ± 3 mm/min (Olesen *et al.*, 1981; Lauritzen *et al.*, 1983), which corresponds to the rate of propagation of spreading depolarization waves (Lauritzen, 1994). In the oligaemic region of migraine patients, blood flow responses to stimulation are also attenuated, suggesting that spreading depolarization is the physiological phenomenon behind blood flow changes (Lauritzen *et al.*, 1983; Hadjikhani *et al.*, 2001). Therefore, it is important to look for new mechanisms that may explain the persistent attenuation of cortical blood vessels response during and after spreading depolarization. These mechanisms are still incompletely understood, partly because our understanding of cerebrovascular control is limited.

Traditionally, brain blood flow regulation was thought to occur at the arteriole level, but it is now clear that regulation of cerebral blood flow can occur at the capillary level (Peppiatt *et al.*, 2006; Dai *et al.*, 2009, 2011; Fernandez-Klett and Priller, 2015; Montagne *et al.*, 2015; Biesecker *et al.*, 2016; Mishra *et al.*, 2016; Kisler *et al.*, 2017). Pericytes cover capillaries and are in direct contact with astrocyte end-feet and endothelial cells (Armulik *et al.*, 2011; Hartmann *et al.*, 2015), contributing to the development and maintenance of the blood–brain barrier (Armulik *et al.*, 2010; Daneman *et al.*, 2010) and the brain's immune response (Yemisci *et al.*, 2009; Kamouchi *et al.*, 2011). The recent development of transgenic mice that express fluorescent markers in pericytes (Zhu *et al.*, 2008) has allowed several *in vivo* studies to demonstrate the contractility of pericytes and how they regulate capillary diameter and cerebral blood flow in both a healthy state and disease (Hall *et al.*, 2014; Kisler *et al.*, 2017). However, the role of brain capillaries and pericytes in the persistent decrease in cerebral blood flow and impaired functional hyperaemia after spreading depolarization has not yet been explored.

In the present study, we tested the hypothesis that vascular disturbances during spreading depolarization are linked to changes in capillary diameter and pericyte calcium responses. Using two-photon microscopy, we imaged mice expressing a fluorescent indicator in pericytes and compared the changes in vascular diameter of penetrating arterioles and first to third order capillaries. During spreading depolarization, significant changes in diameter were detected not only in penetrating arterioles, but also in capillaries up to the third order. Using a genetically encoded calcium indicator, we recorded intracellular calcium changes in pericytes and vascular smooth muscle cells. The long-lasting capillary constriction after spreading depolarization was coupled to a large increase in pericyte cytosolic calcium. After spreading depolarization, we assessed the somatosensory stimulation-induced vascular dilation and found that it was impaired for all vessel orders. Moreover, the calcium responses to stimulation were impaired after spreading depolarization, suggesting that pericyte dysfunction is partly responsible for the impairment of brain hyperaemia. In conclusion, we demonstrate an active role of capillary pericytes in physiology and in spreading depolarization. Our findings provide a novel pathophysiological mechanism for patients with migraine with aura.

Materials and methods

Animal handling

All procedures involving animals were approved by the Danish National Ethics Committee according to the guidelines set forth in the European Council's Convention for the Protection of Vertebrate Animals Used for Experimental and Other Scientific Purposes and are in compliance with the ARRIVE guidelines. Twenty 10 to 15-week-old male Tg(Cspg4-DsRed.T1)1Akik (called DsRed NG2 in the text and figures) mice purchased from the Jackson Laboratory and bred in-house were examined in the present study.

PDGFβr GCaMP6s adeno-associated virus

To generate adeno-associated virus 2/5 (AAV2/5) capable of expressing the calcium indicator GCaMP6s in pericytes and vascular smooth muscle cells, we inserted the *Pdgfrb* promoter (herein PDGFβr) from mice (Mellgren *et al.*, 2008) into a pZac2.1 plasmid. The GCaMP6s construct was cloned into the SalI and BamHI sites downstream of the *Pdgfrb* promoter to generate plasmids called pZac2.1 PDGFβr GCaMP6s. The fully sequenced plasmids were sent to the Penn Vector Core, which generated AAV2/5 for each construct at a concentration of $\sim 2 \times 10^{13}$ genome copies per millilitre (gc/ml).

Surgery and *in vivo* microinjections

Male DsRed NG2 mice were prepared for virus microinjection on postnatal Day 46–67 (P46–P67). All surgical procedures

were conducted under general anaesthesia using continuous isoflurane (induction at 5% and maintenance at 1–2.5%, vol/vol). The depth of anaesthesia was monitored continuously and adjusted when necessary. After inducing anaesthesia, the mice were fitted into a stereotaxic frame, with their heads secured by blunt ear bars and their noses placed into an anaesthesia and ventilation system. The mice were administered 0.05 ml of carprofen (Rimadyl®; 0.1 mg/ml; Pfizer) and 1 ml of sterile saline subcutaneously before surgery. The surgical incision site was cleaned three times with disinfecting wipes. Skin incisions were followed by a craniotomy 1–2 mm in diameter next to the right somatosensory cortex using a high-speed drill. Saline was applied to the skull to reduce heating caused by drilling. Unilateral viral injections were performed using a stereotaxic apparatus to guide the placement of the microsyringe next to the right barrel cortex (1 mm posterior to bregma, 1 mm lateral to midline, and 300 µm from the pial surface). A total of 1 µl of pZac2.1 PDGFβr GCaMP6s (2.4×10^{13} gc/ml) was injected at a rate of 150 nl/min using a syringe pump. The microsyringe was left in place for 10 min after the injection was finished. Surgical wounds were closed with veterinary glue. After surgery, animals were allowed to recover overnight in cages placed partially on a heating pad. Rimadyl® was administered twice per day for up to 2 days after surgery.

Surgical procedures for imaging

Fourteen to 21 days after virus injection, the mice were surgically prepared for imaging. Anaesthesia was induced with bolus injections of xylazine [10 mg/kg intraperitoneally (i.p.)] and ketamine (60 mg/kg i.p.) and maintained during surgery with supplemental doses of ketamine (30 mg/kg/20 min i.p.). Upon completion of all surgical procedures, the anaesthesia was switched to α-chloralose (50 mg/kg/h intravenously). The trachea was cannulated for mechanical ventilation (MiniVent model 845, Harvard Apparatus). Catheters were placed into the left femoral artery and vein for the infusion of substances, blood pressure monitoring, and blood gas sampling. To ensure that the animals were kept under physiological conditions, end-expiratory CO_2 and blood pressure were monitored continuously. Blood gases were assessed in arterial blood samples (pO_2, 95–110 mmHg; pCO_2, 35–40 mmHg; pH, 7.35–7.45) using an ABL 700Series Radiometer. A craniotomy with a diameter of ~3 mm was drilled, centred at 0.5 mm behind and 3 mm to the right of bregma over the somatosensory barrel cortex region and overlapping the craniotomy made for virus injection. After removal of the dura, the cortex was covered with 0.75% agarose gel and moistened with artificial CSF (pH 7.4 at 34°C). Part of the craniotomy was covered with a glass coverslip to allow imaging, and the remaining part of the craniotomy permitted insertion of a glass microelectrode. Changes in vessel diameter and cytosolic calcium responses from pericytes in response to whisker pad stimulation or spreading depolarization were examined using two-photon microscopy. At the end of the experiments, mice were euthanized by intravenous injection of pentobarbital followed by decapitation.

Spreading depolarization and whisker pad stimulation

The mouse barrel cortex was activated by stimulation of the contralateral ramus infraorbitalis of the trigeminal nerve using a set of custom-made bipolar electrodes inserted percutaneously. The stimulation pulse-width was 1 ms at 1.5 mA and in trains of 15 s at 2.0 Hz. During whisker stimulation, we did not observe a change in blood pressure, (-0.10 ± 0.13% of pre-stimulation baseline, $P = 0.43$ with paired t-test) when comparing baseline and stimulation period for 20 stimulations in 10 animals). Electrocorticography (ECoG) and the direct current (DC) were monitored using a single-barrel glass microelectrode filled with isotonic NaCl. The DC was obtained by using a differential amplifier (gain, 10×; bandwidth, 0.1–10 000 Hz; DP-311 Warner Instruments). The spreading depolarization was monitored in the sensory cortex as a depression of the spontaneous ECoG signal and as a negative shift in DC potential. To trigger spreading depolarization, a second craniotomy was drilled over the lateral parietal cortex, posterior to the first (2 mm behind bregma, 2 mm to the right of bregma). Potassium acetate (KAc, 0.5 M) was pressure injected into the cortex. The injected volume was estimated to 1–2 µl of KAc and did not cause a lesion (bleeding or tissue damage) in the brain, but triggered spreading depolarization. A second spreading depolarization was elicited at least 45 min after the first one, a time period long enough to allow the cerebral blood flow to return to baseline (Ayata and Lauritzen, 2015; Khennouf *et al.*, 2016). To ensure that no spreading depolarization was triggered during surgical preparation, our technique for making craniotomies has previously been validated. By measuring cerebral blood flow while drilling the craniotomy, we could show that no spreading depolarization was elicited (Khennouf *et al.*, 2016). Moreover, prior to our first spreading depolarization we measure whisker responses, and mice that did not show normal vessel diameter responses to stimulation were discarded from the dataset, ensuring that no spreading depolarization were triggered before recordings started.

Two-photon imaging

Calcium and vessel imaging was performed using a commercial laser scanning multiphoton excitation system (FluoView FVMPE-RS, Olympus) and a Mai Tai HP Ti:Sapphire laser (Millennia Pro, Spectra Physics) with a 25 × 1.05 NA-water-immersion objective (Olympus). The excitation wavelength was set to 920 nm. The frame resolution was 0.275 µm/pixel with a 512 × 512 pixels frame during spreading depolarization imaging and 512 × 384 pixels frame during whisker stimulation imaging. Images were taken at a speed of 1.09 frames per second during spreading depolarization and 8.13 frames per second during whisker stimulation. After a vessel branching from the penetrating arteriole to a third order capillary was found, a z-stack was recorded followed by time-lapse imaging with somatosensory stimulation. This was repeated for three different vessel trees per animal. Spreading depolarization was imaged in one vessel branching from the penetrating arteriole to a third order capillary in a single plane. If a shift in the z-plane occurred during the spreading depolarization episode due to tissue swelling, the recording was discarded from the analysis.

The *z*-stack of this vessel tree was recorded prior to spreading depolarization and 15 and 30 min after spreading depolarization. Two spreading depolarization episodes were imaged per animal. Twenty minutes after spreading depolarization, the whisker stimulation was repeated and imaged in three vessel trees. At no time was any tissue exposed to power above 20 mW, and no signs of photo-toxicity were observed. Pericytes were localized using DsRed fluorescence as described previously (Hall *et al.*, 2014). To label the blood plasma, 2% (wt/vol) FICT-dextran was administered via the venous catheter. No dye was injected during imaging of calcium signal to avoid contamination of the GCaMP6s signal from the FITC signal. The calcium activity was imaged in pericyte cell bodies located on first, second, and third order capillaries and in vascular smooth muscle cells surrounding the penetrating arterioles using GCaMP6s fluorescence.

Calcium and vessel diameter measurement

We selected regions of interest to extract the calcium signals only on structures exhibiting both DsRed and GCaMP6s fluorescence. Regions of interest were placed on the tissue surrounding penetrating arterioles or on the cell bodies of pericytes from first to third order capillaries. At every time point during stimulation, the evoked calcium fluorescence signal (FS) was monitored and expressed as a percentage of pre-stimulation baseline [F0; $\Delta F = (FS - F0) \times 100 / F0$]. The calcium response was defined as the peak value or area under the curve of the normalized fluorescence signal during whisker stimulation and spreading depolarization. To measure vessel diameters, lines were placed perpendicular across penetrating arterioles and first to third order capillaries, at pericyte cell bodies or processes, as shown in Fig. 1B. To measure vessel diameter, we used custom software with codes available from the libraries https://github.com/abrazhe/image-funcut/tree/develop, https://github.com/drkutuzov/BioTimeLapse. In short, shifts in the *x*–*y* plane were corrected and blood vessel boundaries were traced on the stabilized time lapse using a restricted active contours approach minimizing local Chan–Vese-based function (Chan and Vese, 2001).

Inclusion of data

During spreading depolarization, if any shift was observed in the *z*-plane the spreading depolarization data were discarded. During spreading depolarization, 20 penetrating arterioles, 20 first order capillaries at cell bodies, 18 first order capillaries at processes, 12 second order capillaries at cell bodies, 11 second order capillaries at processes, seven third order capillaries at cell bodies, and seven third order capillaries at processes were then analysed from 20 spreading depolarizations. During whisker stimulation, if the penetrating arteriole was responding to stimulation or spreading depolarization, then all other branches were included as responders. Twenty-nine penetrating arterioles, 29 first order capillaries at cell bodies, 21 first order capillaries at processes, 19 second order capillaries at cell bodies, 20 second order capillaries at processes, 17 third order capillaries at cell bodies, and 17 third order capillaries at processes were analysed. During calcium measurement of vascular smooth muscle cells and pericytes, the GCaMP6s signal was extracted only when it showed a different signal than the DsRed fluorescence signal, to ensure that no artefacts due to an increase of vessel diameter were included. Spreading depolarization does not always evoke an initial vasoconstriction (phase 1), but when it does, this phase is often associated with strong vasomotion during a short period of time. This vasomotion often triggers a shift in the *z*-plane and hence makes two-photon measurements difficult. Therefore, due to the low occurrence of the initial constriction of the spreading depolarization and its large *z*-plane movement, we did not include calcium measurements during phase 1. The dilation and long-lasting constriction seen during phases 2 and 3 are longer and not as abrupt, allowing more stable measurements. Before performing statistical tests, a ROUT test using a false discovery rate of Q = 1% was performed to discard remaining outliers. This test only discarded one outlier, a measurement of a second order capillary during the dilation phase of spreading depolarization.

Statistical analysis

The differences between the first and second spreading depolarization, and before and after spreading depolarization for whisker stimulations were determined using two-way ANOVA with the significance level set at $\alpha = 0.05$. To evaluate whether a vessel was responding during spreading depolarization or whisker stimulation, we used one-way ANOVA. Data were compared to a 60-s pre-spreading depolarization or 15-s pre-stimulation baseline and the significance level set at $\alpha = 0.01$. When $P < 0.01$, the Sidak *post hoc* test was used to assess which vessel type was responding. We also used one-way ANOVA to assess the difference in diameter changes between different vessel types during spreading depolarization or whisker stimulation with the significance level set at $\alpha = 0.05$. The Sidak *post hoc* test was then used to compare the extent of the diameter change in penetrating arterioles to first order capillaries at pericyte cell bodies, or for all vessel orders to compare diameters at pericyte cell bodies versus pericyte processes.

Results

Spreading depolarization was induced by a microinjection of 0.5 M potassium acetate 5 mm from the recording site (Fig. 1A). Spreading depolarization evokes changes on the cerebral vasculature that has been described in three phases. During phase I, vessels exhibits mild constriction with a decrease in blood flow, followed by a large dilation and blood flow increase during phase II. Finally, a long-lasting constriction and blood flow decrease occurs during phase III (Ayata and Lauritzen, 2015; Khennouf *et al.*, 2016). In the present study, the phases were defined between times when the penetrating arteriole diameter went back to the pre-spreading depolarization baseline (Fig. 2). A second spreading depolarization was induced 45 min after the first. We did not find any significant difference between the vessel diameter changes after the first spreading depolarization compared to the second spreading depolarization during phase I ($P = 0.33$, two-way ANOVA; Supplementary Fig. 1A), phase II ($P = 0.93$, two-way

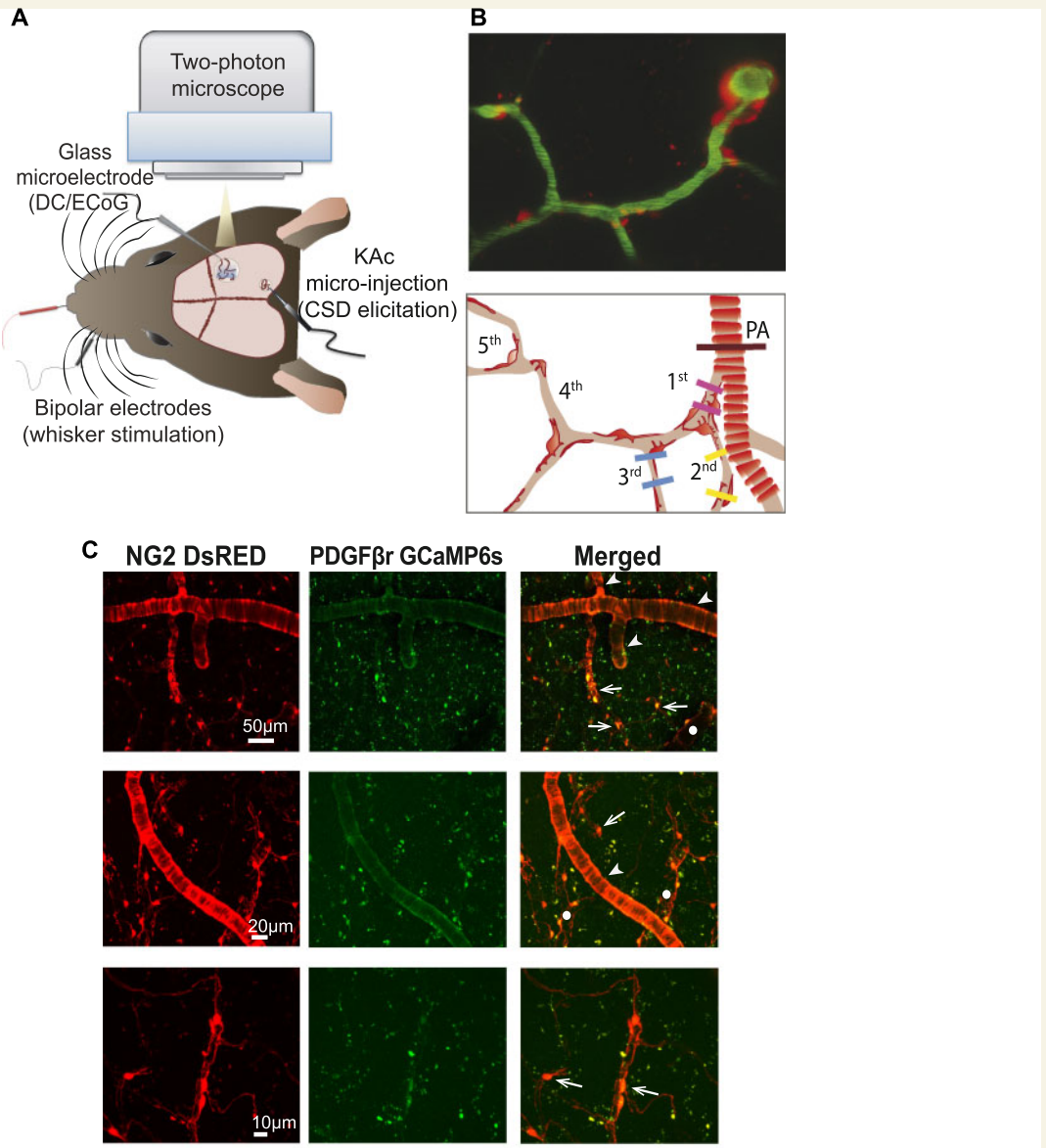

Figure 1 Experimental design. (**A**) Mouse head viewed from above. Spreading depolarization was elicited in the posterior part of the somatosensory cortex by microinjecting potassium acetate (KAc). Spreading depolarization propagated through the barrel cortex and was monitored via electrocorticography (ECoG) using a glass microelectrode. The electrode was also used to record the direct current (DC) shift in the barrel cortex, showing the spreading depolarization. Vessel diameter, pericyte fluorescence, and calcium activity were recorded by two-photon microscopy. (**B**) Two-photon microscopy image of the vasculature from a NG2 DsRed mouse cortex (*top*), and schematic illustration of the pericyte and vessel order. The contour-based analysis was performed on penetrating arterioles (brown line) and at first (pink line), second (yellow lines), and third (blue lines) order capillaries at the pericyte cell body and processes. (**C**) Two-photon microscopy images of brain capillary pericytes. Mice with genetically encoded DsRed under the control of the NG2 promoter (red fluorescence, *left*) were injected with an adeno-associated virus (AAV2/5) inducing the transcription of calcium indicator GCaMP6s under the control of the *Pdgfrb*/PDGFβr promoter (green fluorescence, *middle*). Only pericytes exhibiting both DsRed and GCaMP6s fluorescence (*right*) were analysed for calcium signal. Arrows mark capillary pericytes, arrowheads mark pial or penetrating arterioles, and circles indicate venous structures.

ANOVA; Supplementary Fig. 1B), or phase III ($P = 0.27$, two-way ANOVA; Supplementary Fig. 1C). We performed *post hoc* tests to compare each vessel type for the first and second spreading depolarization and found no difference (data not shown). Therefore, we decided to compile the results from both spreading depolarizations.

Spreading depolarization evoked vasculature changes during initial constriction: phase I

In phase I, an initial constriction was observed in 12 of 20 spreading depolarizations in 10 animals. For these animals,

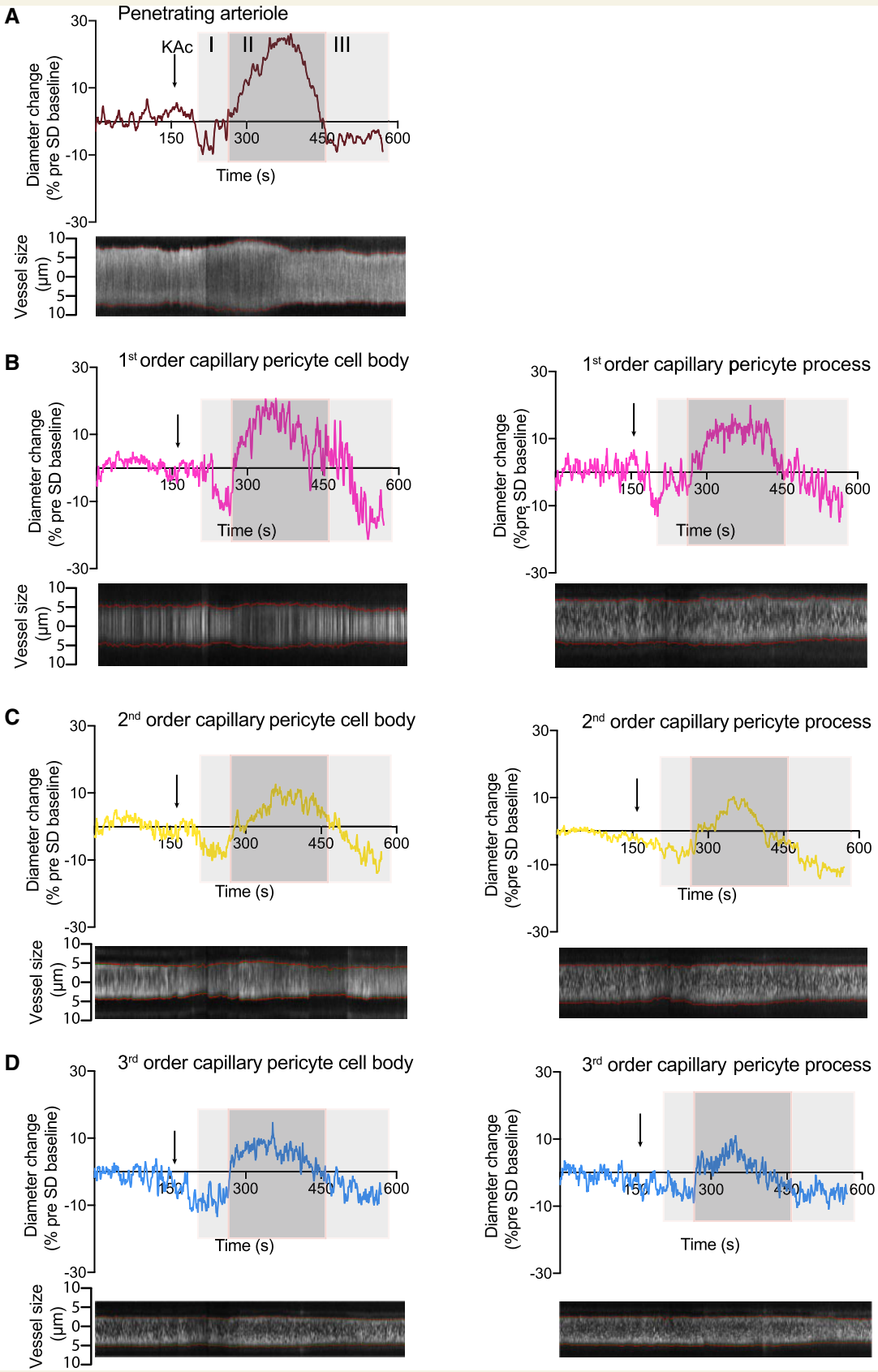

Figure 2 Spreading depolarization evoked changes in vessel diameter. Representative examples of spreading depolarization-induced changes in the diameter of penetrating arterioles (**A**), first (**B**), second (**C**), or third (**D**) order capillaries at the pericyte cell body (*left*) or processes (*right*). Spreading depolarization was triggered by injection of potassium acetate (KAc, black arrow) and evoked changes in the diameters of all types of vessels. These changes were characterized by an initial small vasoconstriction, phase I (light square), followed by a large vasodilation, phase II (dark square), and long-lasting vasoconstriction, phase III (light square). The traces of diameter changes are normalized to a pre-spreading depolarization baseline. The *bottom* images show the contour of the vessel walls using intra-vascular FITC-dextran over the recording period. SD = spreading depolarization.

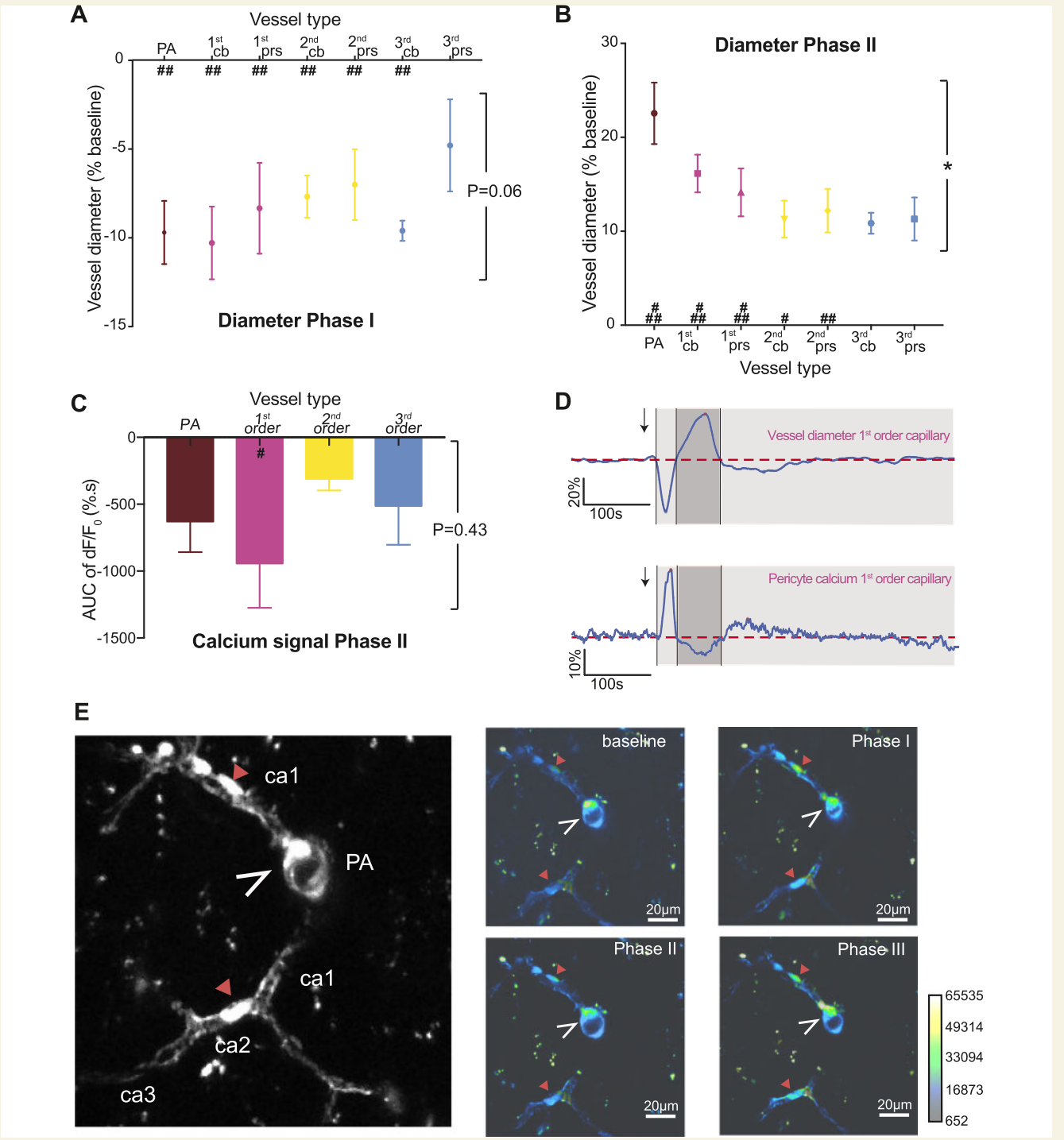

Figure 3 Spreading depolarization evoked changes in vessel diameter and pericyte calcium changes during phases I and II. (**A** and **B**) Measurement of vessel diameter during phases I and II of the spreading depolarization for penetrating arterioles (PA, brown), first (pink), second (yellow), and third (blue) order capillaries at pericyte cell bodies (cb) and processes (prs). All vessels constricted during phase I of the spreading depolarization except for third order capillaries at pericyte processes. During phase II, third order capillaries did not exhibit dilation compared to the pre-spreading depolarization baseline. Values represent the minimum (**A**) or maximum (**B**) vessel diameter as a percentage of pre-spreading depolarization baseline for 12 and 20 spreading depolarizations waves, respectively. (**C**) Average fluorescence intensity of GCaMP6s expressed by pericytes during phase II of spreading depolarization. The negative area under the curve of the fluorescence intensity was normalized to a pre-spreading depolarization baseline for perivascular cells located on penetrating arterioles or first to third order capillaries for six animals. (**D**) Representative example of spreading depolarization-evoked changes in the diameter of a first order capillary (*top*) and calcium fluorescence intensity extracted from a pericyte located on the same vessel (*bottom*). Both traces are normalized to this pre-spreading depolarization baseline (dashed line). (**E**) GCaMP6s fluorescence in capillary pericytes (red arrowheads) and vascular smooth muscle cells around the penetrating arteriole cross section (open white arrowheads). The vascular tree is detailed on the *left*, and *right* panels show the average GCaMP6s fluorescence during baseline period, and phases I, II and III of the spreading depolarization. Data represent the mean ± standard error of the mean (SEM). $^{*}P < 0.05$ using one-way ANOVA; $^{\#\#\#}P < 0.0001$, $^{\#\#}P < 0.001$, $^{\#}P < 0.01$ compared to pre-spreading depolarization baseline with the *post hoc* Sidak test.

the different vessel orders were analysed for diameter changes. Penetrating arterioles, first, second, and third order capillaries (as defined in Fig. 1B) all decreased in diameter during phase I (Fig. 2) by an average of 8.2 ± 1.8% (Fig. 3A). The magnitude of constriction was the same in penetrating arterioles and capillaries ($P = 0.06$, one-way ANOVA; Fig. 3A). To investigate the specific role of pericytes during phase I, the capillary diameter responses compared to baseline were analysed at sites with pericyte cell bodies and pericyte processes. All vessels constricted during phase I of the spreading depolarization ($P < 0.001$) except for third order capillaries at pericyte processes ($P = 0.105$ with Sidak *post hoc* test; Fig. 3A), for which the decrease in diameter localized to pericyte cell bodies but not pericyte processes. This may reflect an overall low responsivity of third order capillaries and that the initial brief vasoconstriction is driven by penetrating arterioles and higher order capillaries.

Spreading depolarization evoked vasculature changes during dilatation: phase II

Following the initial constriction, cortical blood vessels dilated (Figs 2 and 3B). This was observed in all animals. Penetrating arterioles and first and second order capillaries exhibited a significant increase in diameter compared to pre-spreading depolarization baseline, whereas third order capillaries did not ($P = 0.037$ with a Sidak *post hoc* test, third order compared to baseline). The extent of dilation was not the same for every vessel type ($P = 0.0204$ with one-way ANOVA; Fig. 3A); the diameter increase was larger in penetrating arterioles than in first order capillaries (22.6 ± 3.3% versus 16.2 ± 2.0 of pre-spreading depolarization baseline, $P = 0.046$ with Sidak *post hoc* test), second order capillaries (22.6 ± 3.3 versus 11.1 ± 1.8% of pre-spreading depolarization baseline, $P = 0.003$ with Sidak *post hoc* test), or third order capillaries (22.6 ± 3.3% versus 10.7 ± 0.8 of pre-spreading depolarization baseline, $P = 0.033$ with Sidak *post hoc* test). This may suggest that penetrating arterioles and first and second order capillaries are more important than third order capillaries for vasodilation during spreading depolarization. This result is in line with previous studies suggesting that actin-containing pericytes, and consequently the possibility to regulate capillary diameter, decrease with capillary order (Hill *et al.*, 2015; Wei *et al.*, 2016; Kisler *et al.*, 2017). The number of pericytes positive for actin has been reported to decrease from 75% to 21.5% from second to third order capillaries (Wei *et al.*, 2016).

We measured the calcium changes in pericytes during phase II of spreading depolarization. For this purpose, we engineered a new adeno-associated virus encoding GCaMP6s under the control of the *Pdgfrb*/PDGFβr promoter in pericytes. We chose GCaMP6s as the calcium indicator because of its high sensitivity (Chen *et al.*, 2013) and PDGFβr for its high specificity for pericyte-specific expression (Hartmann *et al.*, 2015; Wei *et al.*, 2016). To confirm that GCaMP6s was expressed in pericytes, we injected the virus into mice expressing the DsRed fluorescent marker in pericytes and vascular smooth muscle cells under the control of the NG2 promoter (Zhu *et al.*, 2008). Only cells demonstrating co-localization of GCaMP6s and DsRed were analysed (Fig. 1C). GCaMP6s was expressed in perivascular cells, with clear fluorescence in pericytes. GCaMP6s was also detected in vascular smooth muscle cells around arterioles (Fig. 1C). This gave us an opportunity to simultaneously analyse changes in the activity of vascular smooth muscle cells surrounding penetrating arterioles and pericytes on capillaries. The analysis showed that an increase in vessel diameter (Fig. 3D) was accompanied by a decrease in calcium fluorescence (Fig. 3C–E and Supplementary Video 1). The largest decrease in calcium was observed in pericytes located on first order capillaries ($P = 0.0014$ compared to pre-spreading depolarization baseline using Sidak *post hoc* test; Fig. 3C–E), followed by vascular smooth muscle cells of penetrating arterioles ($P = 0.037$ compared to pre-spreading depolarization baseline using Sidak *post hoc* test). Even though pericytes located on second and third order capillaries exhibited a decrease in calcium, as indicated by the area under the curve below zero during the spreading depolarization-evoked dilation, we found no significant difference compared to the pre-spreading depolarization calcium baseline ($P = 0.32$ and 0.17, respectively, in a *post hoc* Sidak test). Taken together, these results indicate that spreading depolarization evokes changes in vascular smooth muscle and pericyte calcium levels that are reflected in changes in the diameters of penetrating arterioles and capillaries. The larger calcium responses in first order capillary pericytes compared to pericytes on second and third order capillaries suggest a more active role of pericytes at low order capillaries compared to higher order capillaries.

Spreading depolarization evoked changes in long-lasting constriction: phase III

Under otherwise physiological conditions, the spreading depolarization-induced hyperaemia is followed by a long-lasting oligaemia (Ayata and Lauritzen, 2015) (Fig. 2). In the present study, the spreading depolarization-induced diameter changes were analysed by extracting the minimum diameter for each type of vessel during the first 9 min after spreading depolarization. Both penetrating arterioles and capillaries responded with constriction ($P < 0.001$ for third order capillaries at pericyte processes and $P < 0.0001$ for all other vessels compared to the pre-spreading depolarization baseline using a Sidak *post hoc* test; Fig. 4A). We compared the response size between vessel types and found that the maximum constriction was dependent on the vessel order ($P = 0.0015$;

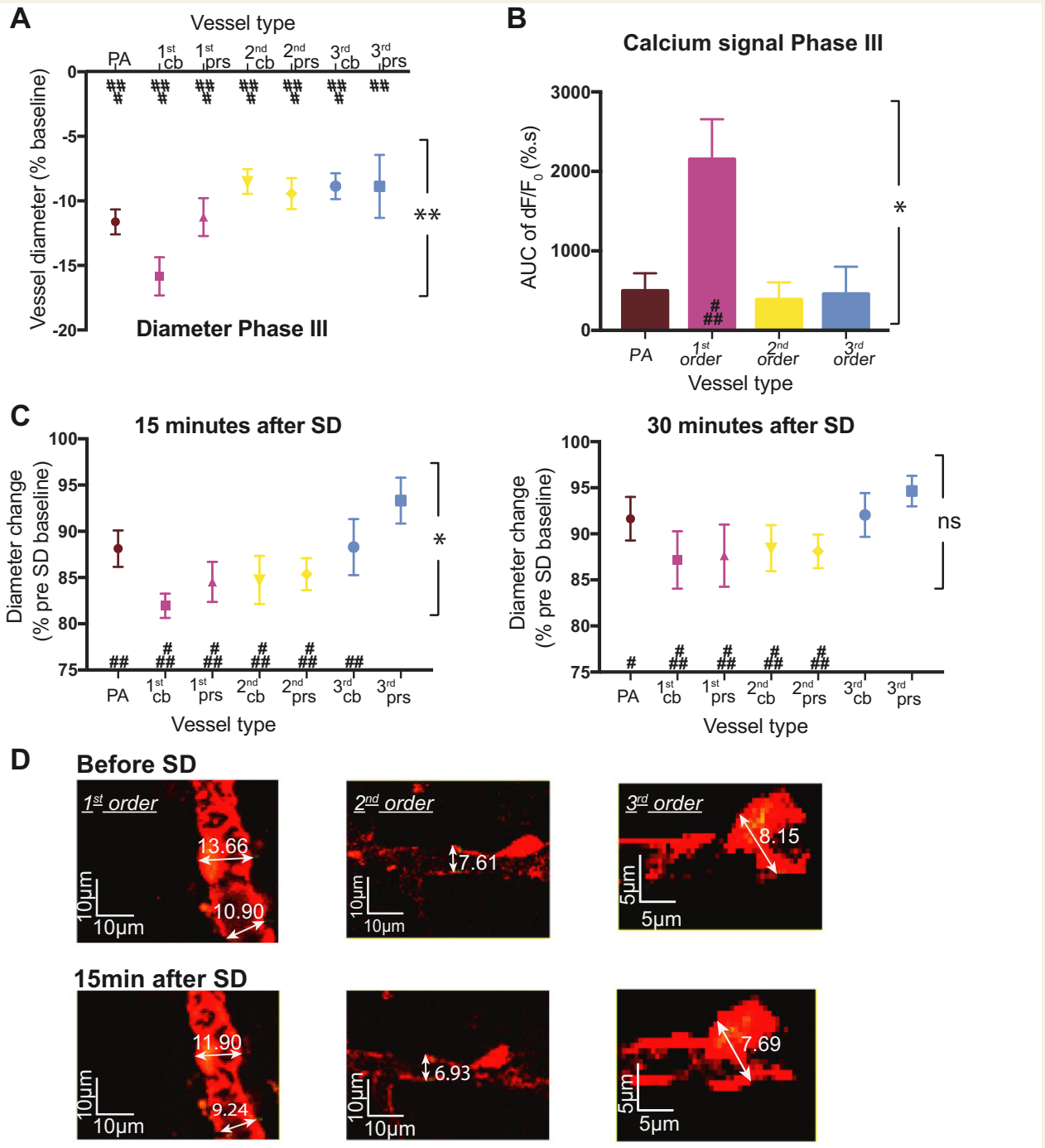

Figure 4 The long-lasting constriction of spreading depolarization is the strongest at first order capillaries. (**A**) Measurement of vessel diameter during phase III of spreading depolarization for penetrating arterioles (PA, brown), first (pink), second (yellow), and third (blue) order capillaries at pericyte cell bodies (cb) and processes (prs). All vessels constricted but the greatest reduction in diameter was for first order capillaries at pericyte cell bodies. Values represent the minimum vessel diameter during the constriction period as a percentage of pre-spreading depolarization baseline for 20 spreading depolarization waves. (**B**) The positive area under the curve (AUC) during phase III was extracted for the fluorescence intensity and normalized to a pre-spreading depolarization baseline. The graph shows calcium fluorescence for vascular smooth muscle cells located on penetrating arterioles (PA, brown) and pericytes on first (pink), second (yellow), or third (blue) order capillaries for six animals. (**C**) The vessel diameter was measured on z-projections of the vascular tree 15 min after spreading depolarization (*left*) for $n = 18$ and 30 min after spreading depolarization (*right*) for $n = 14$. Values are normalized to the measurement made on the pre-spreading depolarization z-projection. (**D**) Magnification of two-photon microscopy images of the z-projection of the vascular tree, with pericytes expressing DsRed protein and appearing in red on first order (*left*), second order (*middle*), and third order (*right*) capillaries before spreading depolarization (*top*) and 15 min after spreading depolarization (*bottom*). Data represent the mean ± SEM. $^{**}P < 0.01$, $^{*}P < 0.05$ using one-way ANOVA; $^{\#\#\#\#}P < 0.0001$, $^{\#\#}P < 0.001$, $^{\#}P < 0.01$ compared to pre-spreading depolarization baseline with *post hoc* Sidak test.

Fig. 4A). Specifically, first order capillaries at pericyte cell bodies constricted more than penetrating arterioles ($-15.8 \pm 1.8\%$ versus -11.7 ± 0.75 of pre-spreading depolarization baseline, $P = 0.0232$ using Sidak's *post hoc* test). First order capillaries also constricted more than second and third order capillaries at pericyte cell bodies ($-15.8 \pm 1.8\%$ versus $-8.5 \pm 1.0\%$ or $-9.4 \pm 2.0\%$, respectively, of pre-spreading depolarization baseline, $P = 0.0003$ and $P = 0.031$ using Sidak's *post hoc* test). Taken together, these results suggest a key role of pericytes on first order capillaries in the long-lasting oligaemia following spreading depolarization. To investigate the role of first order capillary pericytes further, we examined whether capillary constriction is congruent with the localization of pericyte cell bodies or processes (Fig. 4A). The data suggest that the diameter of first order capillaries decreased more at pericyte cell bodies than pericyte processes ($-15.8 \pm 1.5\%$ versus $-11.3 \pm 1.5\%$, $P = 0.0164$ using Sidak's *post hoc* test).

The vasoconstriction was accompanied by an increase in perivascular calcium fluorescence, with the largest increase in intracellular calcium occurring in pericytes on first order capillaries ($P < 0.0001$ compared to the pre-spreading depolarization fluorescence). Although the fluorescence intensity increased in pericytes located on other vessels, the total calcium signal (calculated as area under the curve) was not significantly different from pre-spreading depolarization fluorescence ($P = 0.20$ at penetrating arterioles, $P = 0.32$ at second order capillaries, and $P = 0.27$ at third order capillaries using a Sidak *post hoc* test; Fig. 4B).

Finally, to assess the full period of constriction, we analysed *z*-stacks of the vasculature before spreading depolarization and 15 min and 30 min after spreading depolarization. We compared the size of the vessels for the same location (Fig. 4D). Fifteen minutes after spreading depolarization, all vessels were constricted compared to before spreading depolarization except for third order capillaries at pericyte processes, which is similar to the pre-spreading depolarization baseline diameter ($P = 0.122$; Fig. 4C, left panel). The extent of constriction differed for different vessel types ($P = 0.037$ with one-way ANOVA); first order capillaries at pericyte cell bodies had the strongest constriction, but the Sidak *post hoc* test did not reveal any difference from penetrating arterioles ($-18.04 \pm 1.3\%$ versus $-11.9 \pm 2.0\%$ of pre-spreading depolarization baseline, $P = 0.095$). Thirty minutes after spreading depolarization, the diameters of third order capillaries at pericyte cell bodies were not different from pre-spreading depolarization values. We found no overall difference in the extent of constriction between vessel types ($P = 0.45$ with one-way ANOVA). Taken together, these results suggest a predominant role of first order capillaries and their pericytes in blood flow regulation during phase III; not only do these capillaries constrict more, but the capillary constriction lasted longer. Moreover, pericytes located on first order capillaries exhibited a persistent increase in calcium during vasoconstriction.

Somatosensory stimulation

We also evaluated the role of capillaries and pericytes in the impairment of brain hyperaemia after spreading depolarization. First, we assessed stimulation-induced changes in vessel diameter for penetrating arterioles, first, second, and third order capillaries at pericyte cell bodies or processes before and 20 min after spreading depolarization. Infraorbital (whisker) stimulations at 2 Hz were performed for a duration of 15 s. In line with previous studies (Hall *et al.*, 2014; Kisler *et al.*, 2017), both penetrating arterioles and capillaries dilated during whisker stimulation (Fig. 5). We found an overall difference in the extent of dilation during stimulation for the different vessels ($P = 0.001$ with a one-way ANOVA; Fig. 5A), but the Sidak *post hoc* test did not reveal any significant difference between the dilation of first order capillaries at pericyte cell bodies and penetrating arterioles ($10.9 \pm 1.4\%$ versus $9.9 \pm 0.8\%$ of pre-stimulation baseline, $P = 0.9$; Fig. 5B and C). Third order capillaries dilated less during stimulation than penetrating arterioles ($6.0 \pm 1.0\%$ versus $9.9 \pm 0.8\%$, $P = 0.03$; Fig. 5B and E) or first order capillaries ($6.0 \pm 1.0\%$ versus $10.9 \pm 1.4\%$, $P = 0.009$; Fig. 5C and E). This result could reflect the level of actin found in pericytes according to the order of capillaries (Hill *et al.*, 2015; Wei *et al.*, 2016). Finally, we examined the GCaMP6s calcium signal in pericytes on capillaries and vascular smooth muscle cells around penetrating arterioles during stimulation (Fig. 6). The signal was quantified to determine the peak values during the 15-s stimulation (Fig. 6A) and the area under the curve for the stimulation and 60 s after (Supplementary Fig. 2). Before spreading depolarization, the stimulation-induced calcium signal decreased significantly in pericytes and vascular smooth muscle cells compared to the pre-stimulation baseline (Fig. 6A and B–E, left panels), and this decrease was more pronounced in pericytes located on first order capillaries than in vascular smooth muscle cells around penetrating arterioles ($-7.8 \pm 1.1\%$ of pre-stimulation baseline for first order pericytes versus $-4.2 \pm 0.8\%$ for penetrating arterioles, $P = 0.03$ with Sidak's *post hoc* test, Fig. 6A). The area under the curve, which represents the total calcium response evoked by whisker stimulation, showed that the somatosensory stimulation significantly decreased calcium fluorescence in all orders of vessels (Supplementary Fig. 2). Taken together, these results show an active role for both vascular smooth muscle cells around penetrating arterioles and capillary pericytes in blood flow regulation during whisker stimulation via the modulation of intracellular calcium activities.

After spreading depolarization, the barrel cortex was stimulated again. Twenty minutes after spreading depolarization, the stimulation-induced blood vessel dilation was significantly smaller than before spreading depolarization ($P < 0.0001$ with two-way ANOVA; Fig. 5A). The increase in diameter was no longer different from pre-stimulation baseline, and the diameter changes were similar between

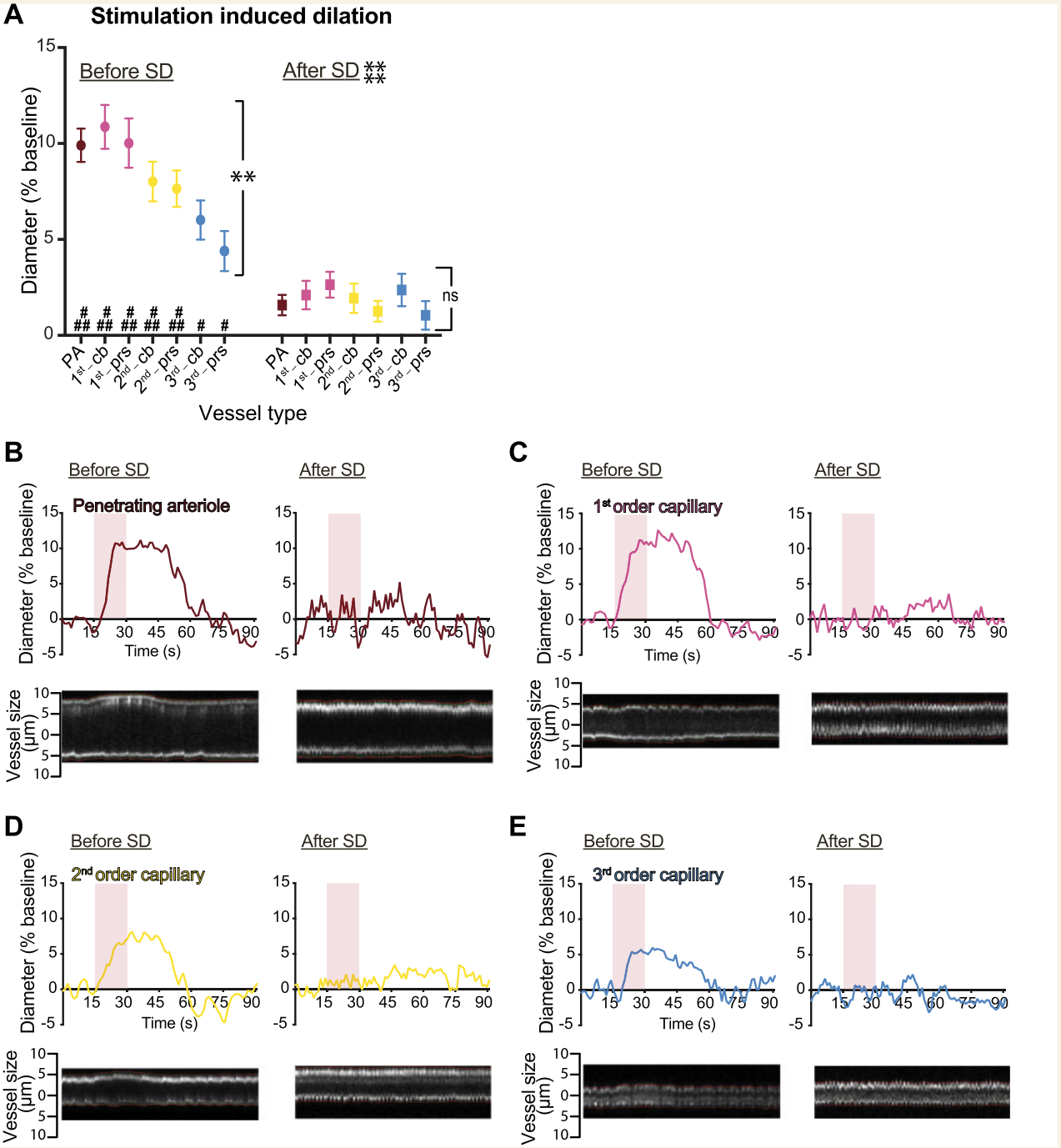

Figure 5 Stimulation-induced dilation is impaired in all vessels after spreading depolarization. (**A**) Measurement of vessel diameter during 15-s, 2-Hz whisker stimulation for penetrating arterioles (PA, brown), first (pink), second (yellow), and third (blue) order capillaries at pericyte cell bodies (cb) and processes (prs) before and 20 min after spreading depolarization. Values represent the maximum vessel diameter during the stimulation period as a percentage of a 15-s pre-stimulation baseline for 12 animals. The dilation was strongest in first order capillaries and penetrating arterioles, but all vessels responded during stimulation compared to the pre-stimulation baseline. After spreading depolarization, none of the vessel types responded. (**B**–**E**) Representative examples of vessel diameter changes during whisker stimulation for penetrating arterioles (**B**), first (**C**), second (**D**), and third (**E**) order capillaries at pericyte cell bodies before (*left*) and 20 min after spreading depolarization (*right*). Raw traces of vessel diameters are shown as a percentage of a 15-s pre-stimulation baseline. The pink square outlines the stimulation period, and the bottom image of the vessel shows the contour of the vessel wall over 90 s. Data represent the mean ± SEM. $^{****}P < 0.0001$, $^{**}P < 0.001$ with two-way ANOVA; $^{\#\#\#\#}P < 0.0001$, $^{\#}P < 0.01$ compared to pre-stimulation baseline with *post hoc* Sidak test. SD = spreading depolarization.

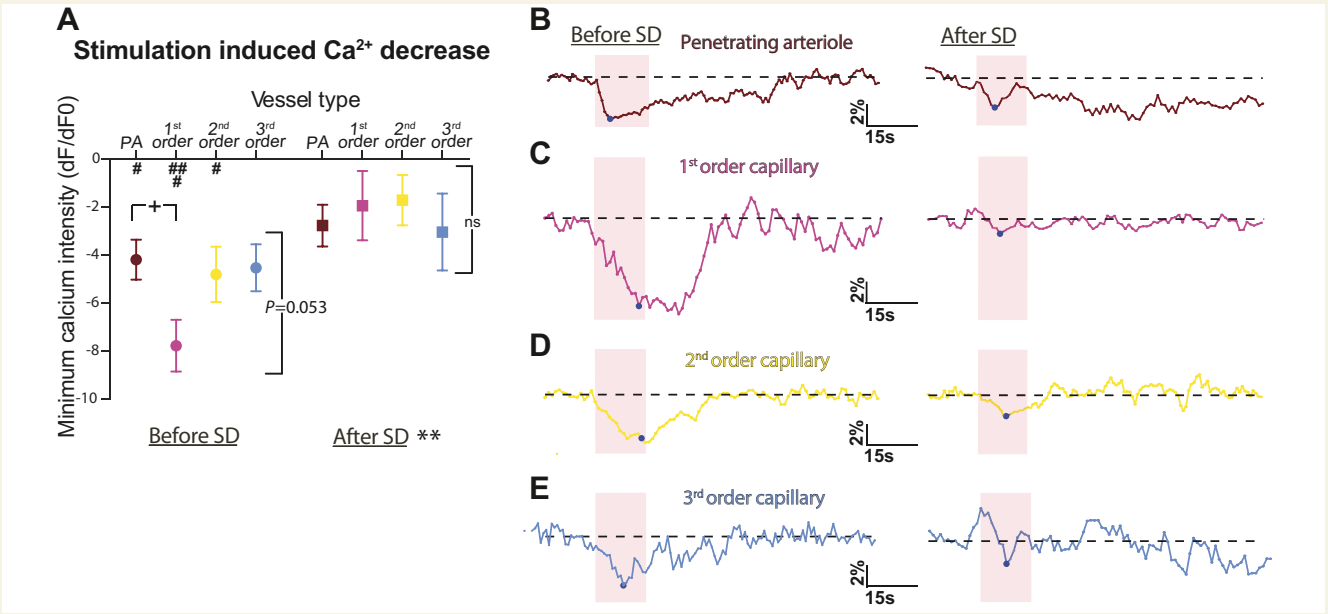

Figure 6 The stimulation-induced decrease in pericyte calcium fluorescence is impaired after spreading depolarization. (**A**) The fluorescence intensity of GCaMP6s expressed by pericytes and vascular smooth muscle cells was extracted and normalized to a 15-s pre-stimulation baseline. The minimum values are shown for vascular smooth muscle cells located on penetrating arterioles (PA, brown) and pericyte cell bodies on first (pink), second (yellow), or third (blue) order capillaries before and 20 min after spreading depolarization for six animals. Vascular smooth muscle cells and pericytes located from penetrating arterioles to second order capillaries responded to stimulation, and the decrease in calcium was larger for pericytes located on first order capillaries. After spreading depolarization, somatosensory stimulation did not induce any change in calcium fluorescence compared to baseline at any vessel branch. (**B**–**E**) Representative examples of the fluorescence intensity of GCaMP6s expressed in pericytes normalized to a 15-s pre-stimulation baseline. The dashed line indicates the baseline and the pink square the 15-s 2-Hz whisker stimulation period. Data are shown for vascular smooth muscle cells located on penetrating arterioles (**B**) and pericyte cell bodies on first (**C**), second (**D**), or third (**E**) order capillaries before (*left*) and 20 min after spreading depolarization (*right*). A blue circle marks the minimum value during stimulation. Data represent the mean ± SEM. $^{**}P < 0.01$, $^{*}P < 0.001$ two-way ANOVA; $^{\#\#\#\#}P < 0.0001$, $^{\#\#\#}P < 0.001$, $^{\#}P < 0.01$ compared to baseline with *post hoc* Sidak test. In **A**, the plus symbol indicates < 0.05, two-tailed *t*-test, comparing values between penetrating arterioles and first order capillaries before spreading depolarization. ns = non-significant; SD = spreading depolarization.

vessel types ($P = 0.68$ for one-way ANOVA; Fig. 5B–E, right panels). This suggests impairment of vessel dilation after spreading depolarization. Finally, we measured calcium fluorescence in pericytes and vascular smooth muscle cells after spreading depolarization. At that point the calcium signal showed a return to pre-spreading depolarization baseline ($-0.8 \pm 0.6\%$ for smooth muscle cells around penetrating arterioles and $2.6 \pm 1.1\%$ for pericytes at first order capillaries, data not shown), suggesting that these cells were at their resting [Ca^{2+}] level. We found a smaller decrease in calcium during stimulation compared to before spreading depolarization ($P = 0.018$ with two-way ANOVA; Fig. 6A and B–E, right panels); the calcium fluorescence signals from pericytes and vascular smooth muscle cells were no longer different from pre-stimulation baseline (Fig. 6A). These results show for the first time the role of pericytes in impaired brain hyperaemia after spreading depolarization. Although previous studies have shown that a small increase in blood flow during stimulation remains after spreading depolarization (Khennouf *et al.*, 2016), we show here that the increase in vessel diameter is impaired for at least 20 min after spreading depolarization. Furthermore, we show that this impairment is not only related to a disruption of neuronal and astrocyte calcium signals after spreading depolarization (Khennouf *et al.*, 2016), but could also be related to a dysregulation of pericyte calcium responses (i.e. capillary dysfunction).

Discussion

The present study characterizes the interplay between the microcirculation and brain pericytes during functional hyperaemia and spreading depolarization, the mechanism of the migraine aura. Somatosensory stimulation evoked dilation in all vessel types, accompanied by a decrease in vascular smooth muscle and pericyte calcium levels. In comparison, spreading depolarization-induced vascular changes were characterized by an initial fast and small constriction (phase I), followed by large vasodilation (phase II) and long-lasting vasoconstriction (phase III). Heterogeneity in the haemodynamic responses has been reported among spreading depolarization studies, with different frameworks of haemodynamic components (Ayata and Lauritzen, 2015). A potential source of this heterogeneity is the difference in the resting vessel diameter caused by difference in

anaesthesia (Ayata and Lauritzen, 2015). In the present study, we cannot exclude a possible effect of α-chloralose on the haemodynamic responses we observed during spreading depolarization. Changes in vascular diameter were observed in penetrating arterioles and capillaries up to the third order during all three phases. Penetrating arterioles dilated more than capillaries during phase II, whereas first order capillaries constricted more than penetrating arterioles during phase III, suggesting a time and phase dependence in the involvement of cortical vessels during spreading depolarization. During vasodilation, spreading depolarization evoked an overall decrease in calcium, whereas the increase in calcium signal during the long-lasting vasoconstriction occurred mainly in pericytes located on first order capillaries. After spreading depolarization, brain hyperaemia was equally impaired for all types of vessels and accompanied by smaller decreases in vascular calcium than before spreading depolarization. Taken together, the data suggest an active role of capillary pericytes during the phase of vasoconstriction after spreading depolarization and for the post-spreading depolarization impairment of functional hyperaemia. The stimulus-driven alterations in pericyte calcium, which accompanied changes in capillary diameter, support a relationship between pericyte calcium activity and the vascular reaction.

Pericytes expressing the fluorescent protein DsRed under the control of the NG2 promoter are recognized by their round cell bodies and long processes and can be located at junctions, where capillaries divide. There is an ongoing debate concerning the identity of pericytes and their subtypes (Hill *et al.*, 2015; Attwell *et al.*, 2016). We have chosen to identify pericytes as cells that are wrapped around capillaries, starting from the first order capillaries (also called pre-capillary arterioles), which have ovoid cell bodies, large processes along the vessels, and appear to be in direct contact with the endothelial cells (Hartmann *et al.*, 2015). Vascular smooth muscle cells around arterioles and oligodendrocytes in the parenchyma also exhibit red fluorescence in NG2-dsRed mice, but vascular smooth muscle cells can be differentiated by their typical ring shape and are unrelated to capillaries. Pericytes cover ∼99% of the capillary bed (Hartmann *et al.*, 2015); therefore, in this study, the trunk of capillaries without pericyte cell bodies was defined as capillaries with pericyte processes. Both vascular smooth muscle cells on penetrating arterioles and pericytes were transfected using our viral construct, which introduced the same genetically encoded calcium indicator into both cell types. This allowed us to examine the interaction between vascular smooth muscle cells and pericytes during physiological stimulation and spreading depolarization.

Capillary dilation responses have been shown to co-localize with pericytes in young adult mice during somatosensory stimulation *in vivo* (Hall *et al.*, 2014) and *in vitro* (Mishra *et al.*, 2016). Furthermore, there is evidence that capillary pericytes contract in response to ATP in brain slices (Peppiatt *et al.*, 2006), and that they can constrict during cerebral ischaemia (Yemisci *et al.*, 2009; Hall *et al.*, 2014). Our findings are consistent with these reports and the suggestion that fluctuations in the intracellular calcium activity of pericytes regulate their contractility and, thus, capillary diameter.

On the other hand, a recent report using NG2-cre transgenic mice expressing channelrhodopsin-2 indicated that optogenetic stimulation led to the constriction of vascular smooth muscle cell-covered arterioles, but not pericyte-covered capillaries (Hill *et al.*, 2015). However, because the authors considered all cells on the capillaries containing actin as vascular smooth muscle cells, it is difficult to directly compare the findings. Vascular smooth muscle cells and pericytes are known to express different types and amounts of contractile proteins (Hill *et al.*, 2015; Wei *et al.*, 2016) and calcium channels (Winkler *et al.*, 2011), and they have been suggested to have different thresholds for stimulation (Kisler *et al.*, 2017). This may explain the different responses to optogenetic stimulation. As we did not use optogenetic stimulation, but rather indirect activation of vascular smooth muscle cells and pericytes via somatosensory stimulation, we did not evaluate the threshold of activation in our study.

Capillary red blood cell slowing, flow arrest, and even transient disappearance of red blood cells from capillary segments have been observed in the first few minutes of spreading depolarization (Chuquet *et al.*, 2007; Ayata, 2009; Unekawa *et al.*, 2015). These findings are consistent with our observation of a brief constriction of penetrating arterioles and first to third order capillaries during phase I of spreading depolarization. This initial constriction is not altered by tetrodotoxin, but is sensitive to the blockade of astroglial calcium waves (Chuquet *et al.*, 2007), suggesting that astrocytes mediate signalling to both capillaries (Lind *et al.*, 2013; Mishra *et al.*, 2016) and arterioles (Gordon *et al.*, 2011) during phase I.

The subsequent increase in cerebral blood flow may be related to the dilation of pial arteries or arterioles close to the brain surface rather than deep penetrating arterioles (Chuquet *et al.*, 2007; Unekawa *et al.*, 2017), or diameter changes in microvessels covered with vascular smooth muscle during the first minutes of spreading depolarization (Hill *et al.*, 2015). In the hyperaemic phase (phase II) of spreading depolarization, we observed the largest dilation in penetrating arterioles and an overall decrease in intracellular calcium fluorescence in vascular smooth muscle cells and pericytes located on first to third order capillaries, which is consistent with previous studies (Chuquet *et al.*, 2007; Unekawa *et al.*, 2017). Although the calcium signal in pericyte of first order capillaries decreased during phase II, the dilation was maximal at penetrating arterioles and decreased with the capillary order. Therefore, we cannot exclude a partial passive dilation from downstream blood pressure in the capillary diameter response during phase II of spreading depolarization.

During the last phase of spreading depolarization, the long-lasting oligaemia (phase III), first order capillaries

demonstrated the greatest constriction and their pericytes the greatest increase in intracellular calcium fluorescence. This suggests an active role of first order capillary pericytes during phase III and is in accordance with a previous study demonstrating that, *in situ*, the intrinsic properties of first order capillary pericytes may exhibit strong and long-lasting constriction due to long-lasting calcium transients (Borysova *et al.*, 2013). Vasoconstrictors can have different effects on vascular smooth muscle cells and pericytes, possibly due to the calcium release via intracellular calcium stores in vascular smooth muscle cells or non-specific cation channels in pericytes (Sakagami *et al.*, 1999). This mechanism could be involved in phase III of spreading depolarization. Our results provide a mechanistic link between vascular changes during spreading depolarization and calcium changes in capillary pericytes or vascular smooth muscle cells.

The present study provides evidence that impaired functional hyperaemia in the wake of spreading depolarization may be the result of reduced calcium responses of vascular smooth muscle cells and pericytes, ultimately leading to a limited oxygen supply (Piilgaard and Lauritzen, 2009; Khennouf *et al.*, 2016). The disruption in vascular smooth muscle and pericyte calcium responses could reflect impaired vasodilator release, which is consistent with our recent finding of reduced stimulation-induced calcium responses in astrocytes and neurons after spreading depolarization (Khennouf *et al.*, 2016).

In summary, we characterized the effect of physiological stimulation and spreading depolarization on cortical penetrating arterioles and capillaries. Our findings of fluctuations in vascular smooth muscle and pericyte calcium during physiological stimulation and spreading depolarization support a direct link between vascular smooth muscle/pericyte contractility and arteriolar/capillary dilation and constriction. Impaired brain hyperaemia after spreading depolarization contributes to prolonged cortical dysfunction in patients with migraine with aura. Prevention of pericyte constriction may reduce the long-lasting decrease in blood flow after spreading depolarization and mitigate cortical dysfunction.

Acknowledgement

We thank Micael Lønstrup for his excellent technical assistance.

Funding

This study was supported by the University of Copenhagen, the NORDEA Foundation Grant to the Center for Healthy Aging at the University of Copenhagen, the Lundbeck Foundation, the NOVO-Nordisk Foundation, and the Danish Medical Research Council. The Khakh lab was funded by the NIH (MH099559).

Supplementary material

Supplementary material is available at *Brain* online.

References

Armulik A, Genove G, Betsholtz C. Pericytes: developmental, physiological, and pathological perspectives, problems, and promises. Dev Cell 2011; 21: 193–215.

Armulik A, Genove G, Mae M, Nisancioglu MH, Wallgard E, Niaudet C, et al. Pericytes regulate the blood-brain barrier. Nature 2010; 468: 557–61.

Attwell D, Mishra A, Hall CN, O'Farrell FM, Dalkara T. What is a pericyte? J Cereb Blood Flow Metab 2016; 36: 451–5.

Ayata C. Spreading depression: from serendipity to targeted therapy in migraine prophylaxis. Cephalalgia 2009; 29: 1095–114.

Ayata C, Lauritzen M. Spreading depression, spreading depolarizations, and the cerebral vasculature. Physiol Rev 2015; 95: 953–93.

Biesecker KR, Srienc AI, Shimoda AM, Agarwal A, Bergles DE, Kofuji P, et al. Glial cell calcium signaling mediates capillary regulation of blood flow in the retina. J Neurosci 2016; 36: 9435–45.

Borysova L, Wray S, Eisner DA, Burdyga T. How calcium signals in myocytes and pericytes are integrated across in situ microvascular networks and control microvascular tone. Cell Calcium 2013; 54: 163–74.

Chan TF, Vese LA. Active contours without edges. IEEE Trans Image Process 2001; 10: 266–77.

Chen TW, Wardill TJ, Sun Y, Pulver SR, Renninger SL, Baohan A, et al. Ultrasensitive fluorescent proteins for imaging neuronal activity. Nature 2013; 499: 295–300.

Chuquet J, Hollender L, Nimchinsky EA. High-resolution *in vivo* imaging of the neurovascular unit during spreading depression. J Neurosci 2007; 27: 4036–44.

Dai M, Nuttall A, Yang Y, Shi X. Visualization and contractile activity of cochlear pericytes in the capillaries of the spiral ligament. Hear Res 2009; 254: 100–7.

Dai M, Yang Y, Shi X. Lactate dilates cochlear capillaries via type V fibrocyte-vessel coupling signaled by nNOS. Am J Physiol Heart Circ Physiol 2011; 301: H1248–54.

Daneman R, Zhou L, Kebede AA, Barres BA. Pericytes are required for blood-brain barrier integrity during embryogenesis. Nature 2010; 468: 562–6.

Dreier JP. Is the blood-brain barrier differentially affected by different variants of migraine? Brain 2016; 139 (Pt 7): 1872–4.

Fernandez-Klett F, Priller J. Diverse functions of pericytes in cerebral blood flow regulation and ischemia. J Cereb Blood Flow Metab 2015; 35: 883–7.

Gordon GR, Howarth C, MacVicar BA. Bidirectional control of arteriole diameter by astrocytes. Exp Physiol 2011; 96: 393–9.

Hadjikhani N, Sanchez Del Rio M, Wu O, Schwartz D, Bakker D, Fischl B, et al. Mechanisms of migraine aura revealed by functional MRI in human visual cortex. Proc Natl Acad Sci USA 2001; 98: 4687–92.

Hall CN, Reynell C, Gesslein B, Hamilton NB, Mishra A, Sutherland BA, et al. Capillary pericytes regulate cerebral blood flow in health and disease. Nature 2014; 508: 55–60.

Hartings JA, Shuttleworth CW, Kirov SA, Ayata C, Hinzman JM, Foreman B, et al. The continuum of spreading depolarizations in acute cortical lesion development: examining Leao's legacy. J Cereb Blood Flow Metab 2017; 37: 1571–94.

Hartmann DA, Underly RG, Grant RI, Watson AN, Lindner V, Shih AY. Pericyte structure and distribution in the cerebral cortex revealed by high-resolution imaging of transgenic mice. Neurophotonics 2015; 2: 041402.

Hill RA, Tong L, Yuan P, Murikinati S, Gupta S, Grutzendler J. Regional blood flow in the normal and ischemic brain is controlled by arteriolar smooth muscle cell contractility and not by capillary pericytes. Neuron 2015; 87: 95–110.

Kamouchi M, Ago T, Kitazono T. Brain pericytes: emerging concepts and functional roles in brain homeostasis. Cell Mol Neurobiol 2011; 31: 175–93.

Khennouf L, Gesslein B, Lind BL, van den Maagdenberg AM, Lauritzen M. Activity-dependent calcium, oxygen, and vascular responses in a mouse model of familial hemiplegic migraine type 1. Ann Neurol 2016; 80: 219–32.

Kisler K, Nelson AR, Rege SV, Ramanathan A, Wang Y, Ahuja A, et al. Pericyte degeneration leads to neurovascular uncoupling and limits oxygen supply to brain. Nat Neurosci 2017; 20: 406–16.

Lauritzen M. Pathophysiology of the migraine aura. The spreading depression theory. Brain 1994; 117(Pt 1): 199–210.

Lauritzen M, Olsen TS, Lassen NA, Paulson OB. Changes in regional cerebral blood-flow during the course of classic migraine attacks. Ann Neurol 1983; 13: 633–41.

Leao AA. Pial circulation and spreading depression activity in the cerebral cortex. J Neurophysiol 1944; 7: 391–6.

Lind BL, Brazhe AR, Jessen SB, Tan FC, Lauritzen MJ. Rapid stimulus-evoked astrocyte Ca2+ elevations and hemodynamic responses in mouse somatosensory cortex *in vivo*. Proc Natl Acad Sci USA 2013; 110: E4678–87.

Mellgren AM, Smith CL, Olsen GS, Eskiocak B, Zhou B, Kazi MN, et al. Platelet-derived growth factor receptor beta signaling is required for efficient epicardial cell migration and development of two distinct coronary vascular smooth muscle cell populations. Circ Res 2008; 103: 1393–401.

Mishra A, Reynolds JP, Chen Y, Gourine AV, Rusakov DA, Attwell D. Astrocytes mediate neurovascular signaling to capillary pericytes but not to arterioles. Nat Neurosci 2016; 19: 1619–27.

Montagne A, Pa J, Zlokovic BV. Vascular plasticity and cognition during normal aging and dementia. JAMA Neurol 2015; 72: 495–6.

Olesen J, Larsen B, Lauritzen M. Focal hyperemia followed by spreading oligemia and impaired activation of rCBF in classic migraine. Ann Neurol 1981; 9: 344–52.

Peppiatt CM, Howarth C, Mobbs P, Attwell D. Bidirectional control of CNS capillary diameter by pericytes. Nature 2006; 443: 700–4.

Piilgaard H, Lauritzen M. Persistent increase in oxygen consumption and impaired neurovascular coupling after spreading depression in rat neocortex. J Cereb Blood Flow Metab 2009; 29: 1517–27.

Sakagami K, Wu DM, Puro DG. Physiology of rat retinal pericytes: modulation of ion channel activity by serum-derived molecules. J Physiol 1999; 521(Pt 3): 637–50.

Sugaya E, Takato M, Noda Y. Neuronal and glial activity during spreading depression in cerebral cortex of cat. J Neurophysiol 1975; 38: 822–41.

Unekawa M, Tomita Y, Masamoto K, Toriumi H, Osada T, Kanno I, et al. Dynamic diameter response of intraparenchymal penetrating arteries during cortical spreading depression and elimination of vasoreactivity to hypercapnia in anesthetized mice. J Cereb Blood Flow Metab 2017; 37: 657–70.

Unekawa M, Tomita Y, Toriumi H, Osada T, Masamoto K, Kawaguchi H, et al. Hyperperfusion counteracted by transient rapid vasoconstriction followed by long-lasting oligemia induced by cortical spreading depression in anesthetized mice. J Cereb Blood Flow Metab 2015; 35: 689–98.

Wei HS, Kang H, Rasheed ID, Zhou S, Lou N, Gershteyn A, et al. Erythrocytes are oxygen-sensing regulators of the cerebral microcirculation. Neuron 2016; 91: 851–62.

Winkler EA, Bell RD, Zlokovic BV. Central nervous system pericytes in health and disease. Nat Neurosci 2011; 14: 1398–405.

Yemisci M, Gursoy-Ozdemir Y, Vural A, Can A, Topalkara K, Dalkara T. Pericyte contraction induced by oxidative-nitrative stress impairs capillary reflow despite successful opening of an occluded cerebral artery. Nat Med 2009; 15: 1031–7.

Zhu X, Bergles DE, Nishiyama A. NG2 cells generate both oligodendrocytes and gray matter astrocytes. Development 2008; 135: 145–57.